

## **Soluble 1:1 Complexes and Insoluble 3:2 Complexes**

Understanding the Phase-Solubility Diagram of Hydrocortisone and  $\gamma$ -Cyclodextrin

Schönbeck, Jens Christian Sidney; Madsen, Tobias Løvgren; Peters, Günther H.; Holm, René; Loftsson, Thorsteinn

*Published in:*  
International Journal of Pharmaceutics

*DOI:*  
[10.1016/j.ijpharm.2017.05.024](https://doi.org/10.1016/j.ijpharm.2017.05.024)

*Publication date:*  
2017

*Document Version*  
Peer reviewed version

*Citation for published version (APA):*

Schönbeck, J. C. S., Madsen, T. L., Peters, G. H., Holm, R., & Loftsson, T. (2017). Soluble 1:1 Complexes and Insoluble 3:2 Complexes: Understanding the Phase-Solubility Diagram of Hydrocortisone and  $\gamma$ -Cyclodextrin. *International Journal of Pharmaceutics*, 531(2), 504-511. <https://doi.org/10.1016/j.ijpharm.2017.05.024>

### **General rights**

Copyright and moral rights for the publications made accessible in the public portal are retained by the authors and/or other copyright owners and it is a condition of accessing publications that users recognise and abide by the legal requirements associated with these rights.

- Users may download and print one copy of any publication from the public portal for the purpose of private study or research.
- You may not further distribute the material or use it for any profit-making activity or commercial gain.
- You may freely distribute the URL identifying the publication in the public portal.

### **Take down policy**

If you believe that this document breaches copyright please contact [rucforsk@kb.dk](mailto:rucforsk@kb.dk) providing details, and we will remove access to the work immediately and investigate your claim.

# **Soluble 1:1 Complexes and Insoluble 3:2 Complexes – Understanding the Phase-Solubility Diagram of Hydrocortisone and $\gamma$ -Cyclodextrin**

Christian Schönbeck<sup>\*,a</sup>, Tobias L. Madsen<sup>b</sup>, Günther H. Peters<sup>b</sup>, René Holm<sup>c</sup>, and Thorsteinn Loftsson<sup>d</sup>.

<sup>a</sup> Department of Science and Environment, Roskilde University, Universitetsvej 1, DK-4000, Roskilde, Denmark

<sup>b</sup> Department of Chemistry, Technical University of Denmark, Building 207, DK-2800 Kongens Lyngby, Denmark

<sup>c</sup> Drug Product Development, Janssen Research and Development, Johnson & Johnson, Turnhoutseweg 30, 2340 Beerse, Belgium

<sup>d</sup> Faculty of Pharmaceutical Sciences, University of Iceland, Hofsvallagata 53, IS-107 Reykjavik, Iceland

\*Corresponding author:

E-mail: [jechsc@ruc.dk](mailto:jechsc@ruc.dk), Telephone: +45 46742345

Department of Science and Environment

Roskilde University

Universitetsvej 1

DK-4000 Roskilde

Denmark

## Abstract

The molecular mechanisms underlying the drug-solubilizing properties of  $\gamma$ -cyclodextrin were explored using hydrocortisone as a model drug. The  $B_S$ -type phase-solubility diagram of hydrocortisone with  $\gamma$ -cyclodextrin was thoroughly characterized by measuring the concentrations of hydrocortisone and  $\gamma$ -cyclodextrin in solution and the solid phase. The drug-solubilizer interaction was also studied by isothermal titration calorimetry from which a precise value of the 1:1 binding constant ( $K_{11} = 4.01 \text{ mM}^{-1}$  at  $20^\circ\text{C}$ ) was obtained. The formation of water-soluble 1:1 complexes is responsible for the initial increase in hydrocortisone solubility while the precipitation of entities with a 3:2 ratio of  $\gamma$ -cyclodextrin:hydrocortisone is responsible for the plateau and the ensuing strong decrease in solubility once all solid hydrocortisone is used up. The complete phase-solubility diagram is well accounted for by a model employing the 1:1 binding constant and the solubility product of the precipitating 3:2 entity ( $K_{32}^S = 5.51 \text{ mM}^5$ ). For such systems, a small surplus of  $\gamma$ -cyclodextrin above the optimum concentration may result in a significant decrease in drug solubility, and the implications for drug formulations are briefly discussed.

Keywords: cyclodextrin; phase-solubility; calorimetry; hydrocortisone; inclusion complex; binding constant

# 1. Introduction

Addition of cyclodextrins (CDs) is an often used formulation strategy to increase the apparent aqueous solubility of poorly soluble drugs (Williams et al., 2013). Formation of water-soluble inclusion complexes between drug and cyclodextrin increases the amount of drug in solution but other mechanisms may also contribute to the increased drug solubility. Both CDs and their complexes may form aggregates in which drug molecules are included, similar to solubilisation of drugs by incorporation into micelles. The exact contribution of CD aggregates to the increased drug solubility is difficult to quantify but it is nevertheless anticipated that aggregate formation can be exploited as a new type of drug delivery system (Ryzhakov et al., 2016). It is clear, however, that a more thorough understanding of the aggregation phenomenon is required.

Hydrocortisone (HC) solubilised by CDs is an often used model system for the study of CD aggregates and their impact on drug solubility (Jansook et al., 2010; Jansook and Loftsson, 2008; Messner et al., 2011a, 2011b; Saokham et al., 2016). In the case of modified cyclodextrins (e.g. hydroxypropylated  $\beta$ - and  $\gamma$ CDs) the equilibrium concentration of hydrocortisone increases linearly with the CD concentration resulting in a so-called  $A_L$ -type phase solubility (PS) diagram, using the classification system of Higuchi and Connors (Higuchi and Connors, 1965). For the natural  $\beta$ - and  $\gamma$ CDs,  $B_S$ -type PS diagrams have been reported which are characterized by an initial linear increase in the amount of dissolved drug followed by a plateau where the concentration of dissolved drug is independent of the CD concentration. After the plateau, the drug concentration decreases with increasing amounts of CD (Figure 1). From a formulation point of view,  $B_S$ -type systems are problematic as just the right amount of CD is required to obtain maximum drug solubility and addition of too much CD (relative to the amount of drug) may significantly lower the amount of dissolved drug. According to the traditional interpretation (Higuchi and Connors, 1965)  $B_S$ -type PS diagrams occur due to formation of complexes with a limited aqueous solubility but more recent

studies suggest that formation of nano- and micrometer-sized aggregates also play an important role (Messner et al., 2011a; Saokham and Loftsson, 2017). However, a detailed mechanistic description involving aggregates has not been provided. The present work aims to fill in this gap *via* a thorough characterization of the system and subsequent modelling of the experimental data.

In order to understand the mechanisms that determine the shape of B<sub>S</sub>-type PS diagrams we have used a novel multifaceted experimental approach combining traditional PS analysis and Isothermal Titration Calorimetry (ITC). As shown in 1965 by Higuchi and Connors, B<sub>S</sub>-type PS diagrams can be analyzed to provide the stoichiometry and binding constant of the formed complexes. More modern techniques are also available to determine the binding constants, e.g. ITC which can provide precise estimates of binding constants and stoichiometries of drug:CD complexes. ITC can normally only be used in the lower concentration range as the technology requires both of the complexing species to be in solution, i.e. the drug solubility in water can define the limitation. So while ITC is very precise for the initial part of the B<sub>S</sub>-type PS diagram it fails in characterizing the following parts where the species are present at higher concentrations. This underlines the importance of multiple characterization approaches for complicated PS diagrams.

Traditionally, PS diagrams are constructed for only one of the components in solution, the drug, and the total concentration of drug in solution is plotted as a function of added CD. Measuring the concentration of the complexing agent is in principle not necessary and is rarely done. However, quantifying the amount of CD in solution allows for a more detailed mechanistic picture in terms of the composition of the precipitate and the identity of the molecular species in solution.

Unfortunately, CDs are not easy to quantify as they contain no chromophores or fluorophores, and researchers have resorted to other analytical techniques, e.g. measuring the refractive index (Jansook et al., 2010). Recently, a method have been developed where the concentration of CDs is determined accurately by HPLC coupled to a Charged Aerosol Detector (Saokham and Loftsson,

2015), thereby assisting the interpretation of the PS diagram. In addition to quantifying the amount of drug and  $\gamma$ CD in solution, we also characterize the overall composition of the precipitate as well as the amount of uncomplexed drug in the precipitate. By combining the information from these complementary analytical techniques we intend to obtain a more complete picture of the molecular mechanisms that determine the features of B<sub>S</sub>-type PS diagrams. Once a mechanistic model is established, it can provide a full map of the formulation space and thereby define the optimal formulation space for a compound with a B<sub>S</sub>-type PS diagram, in the present case HC.

## 2. Theoretical Background

The analysis of  $B_S$ -type phase diagrams was pioneered by Higuchi and Connors in 1965 (Higuchi and Connors, 1965), but a more exhaustive and formal mathematical treatment has later been developed which also takes various higher-order complexes into account (Zughul and Badwan, 1998, 1997; Zughul, 2007).

Complex usually refers to molecular assemblies formed by combination of substrates (S) and ligands (L), and in most cases complex formation is a reversible process. PS diagrams are typically constructed by mixing a constant amount of solid substrate (in this work HC) with a medium containing varying concentrations of solubilizer or ligand,  $L_t$ , (in this work  $\gamma$ CD) and then measuring the equilibrium concentration of dissolved solute,  $S_{eq}$ . If one of the formed complexes has a limited solubility and starts precipitating from the solution above a given concentration of solubilizer  $B_S$ -type diagrams are observed. These are divided into 3 regions as sketched in Figure 1.

Figure 1

**Region I:** Total concentration of solute in solution,  $S_{eq}$ , increases with increasing concentration of solubilizer. Precipitate consists of solid solute.

**Region II:** The solubility limit of one of the formed complexes is exceeded, and the concentrations of all species in solution are constant. Precipitate consists of solid solute and precipitated complexes.

**Region III:** All solid S is depleted and exists as free and complexed S in the solution and as complexed S in the precipitate.  $S_{eq}$  decreases with increasing  $L_t$  due to the gradual conversion of free S and soluble complexes to precipitated complex.

In each of the 3 regions the following mass balances apply for the molecular species in solution:

$$S_{eq} = [S] + [LS] + \dots \quad (1)$$

$$L_{eq} = [L] + [LS] + \dots \quad (2)$$

Where the concentration of 1:1 complexes,  $[LS]$ , is related to the concentrations of free solutes,  $[S]$ , and hosts,  $[L]$ , *via* the equilibrium constant:

$$[LS] = K_{11} \cdot [L] \cdot [S] \quad (3)$$

The (...)’s in equations 1 and 2 represent possible higher-order complexes,  $L_xS_y$ . If these are present, their concentrations are given as:

$$[L_xS_y] = K_{xy} \cdot [L]^x \cdot [S]^y \quad (4)$$

These equations pertain to each of the 3 regions but the mathematical description of the PS diagram requires additional restrictions which are specific to each region. In a standard PS diagram  $S_{eq}$  is plotted *versus* the known initial concentration of ligand,  $L_t$ , in the liquid phase. In order to express  $S_{eq}$  as a function of  $L_t$  it is necessary to restrict some of the variables in equations 1-4. These restrictions are specific to each of the 3 regions:

**Region I:** Solid solute is present, and the concentration of free solute,  $[S]$ , is therefore equal to its intrinsic solubility  $S_0$  (its solubility in the aqueous medium when no ligand (i.e. cyclodextrin) is present). As no host has precipitated,  $L_{eq}$  is equal to the known concentration  $L_t$ .  $S_{eq}$  can therefore be expressed as a function of  $L_{eq}$ , the constant  $S_0$ , and the equilibrium constants.

**Region II:** Solid solute and precipitated complex are present, and so  $[S] = S_0$ , and the concentration of precipitating complex is equal to its solubility,  $S_{XY}$ .  $S_{eq}$  is a function of the constants  $S_0$ ,  $S_{XY}$ , and the complex equilibrium constants and is therefore itself a constant.



**Region III:** Precipitated complex is present and its concentration is equal to its solubility,  $S_{XY}$ . Now there are too many unknowns for the equations to be solved so another requirement has to be introduced:

$$L_t = L_{eq} + x \cdot L_x S_y^{prec}. \quad (5)$$

$$S_t = S_{eq} + y \cdot L_x S_y^{prec}. \quad (6)$$

Subtracting  $x \cdot S_t$  from  $y \cdot L_t$  eliminates the amount of precipitated complex,  $L_x S_y^{prec}$ , and results in:

$$y \cdot L_t - x \cdot S_t = y \cdot L_{eq} - x \cdot S_{eq} \quad (7)$$

Inclusion of equation 7 allows  $S_{eq}$  to be calculated in region III as a function of the variable  $L_t$ , the constants  $S_t$ ,  $S_{XY}$ , and the complex equilibrium constants.

From equations 1-3 and the region-specific requirements the equilibrium concentrations of solute and ligand,  $S_{eq}$  and  $L_{eq}$ , can be expressed as a function of the initial concentration of ligand,  $L_t$ .

These expressions are given in Table 1 for the 1:1 model together with the boundaries between the regions. Plotting these equations produces a theoretical PS diagram with a shape determined by  $S_0$ ,  $S_{11}$ ,  $K$ , and  $S_t$ . Similarly, equations 1-4 may be solved for systems that form higher-order complexes but often they can only be solved numerically. More information on how to solve these equations and construct PS diagrams is provided as Supplementary material.

Table 1 Overview of the equations that constitute the solution to the 1:1 model. The first row shows the starting points of the regions. Region I, for example, starts at  $L_t = 0$  mM and ends at  $L_t = S_{11}(1+1/KS_0)$  where region II sets in.  $\Delta = L_t - S_t$ .

	Region I	Region II	Region III
Onset of region	$L_t = 0$	$L_t = S_{11} \left(1 + \frac{1}{K \cdot S_0}\right)$	$L_t = \frac{S_{11}}{K \cdot S_0} + S_t - S_0$
Equilibrium concentration of solute, $S_{eq}$	$S_0 + L_t \cdot \frac{K \cdot S_0}{K \cdot S_0 + 1}$	$S_0 + S_{11}$	$S_{11} - \frac{\Delta \cdot K - \sqrt{\Delta^2 \cdot K^2 + 4 \cdot S_{11} \cdot K}}{2K}$
Equilibrium concentration of ligand, $L_{eq}$	$L_t$	$S_{11} \left(1 + \frac{1}{K \cdot S_0}\right)$	$S_{11} + \frac{\Delta \cdot K + \sqrt{\Delta^2 \cdot K^2 + 4 \cdot S_{11} \cdot K}}{2K}$

### 3. Materials and Method

#### 3.1 Isothermal Titration Calorimetry (ITC)

ITC experiments were performed on a VP-ITC (Malvern Instruments, Malvern, UK). A solution of 10 mM  $\gamma$ CD (purity  $\geq$  98%, Sigma-Aldrich, St. Louis, MO, USA) in Milli-Q water was injected in 10  $\mu$ L aliquots into a solution of 0.5 mM HC (purity  $\geq$  98%, Sigma-Aldrich) at 10, 25, 40, and 55°C. Heat signals were integrated using the ITC data analysis application for Origin 7.0 that was provided with the calorimeter. The integrated heats and the cell concentrations were exported and analyzed using in-house Matlab scripts to yield the thermodynamic parameters of the complexation equilibrium (Schönbeck et al., 2012).

#### 3.2 Phase Solubility (PS)

Stock solutions of  $\gamma$ CD were made by dissolving  $\gamma$ CD (CycloLab, Hungary) in Milli-Q water. The concentrations were corrected for the water content of the  $\gamma$ CD (10.5% w/w). Approximately 25.4 mg of microcrystalline HC (Fagron, The Netherlands) was added to each of the 4 ml glass vials, corresponding to a concentration of around 35 mM upon addition of 2 ml of solvent of varying concentrations of  $\gamma$ CD in the range 0-140 mM. The mixtures were sonicated for 40 minutes at 60°C and left to equilibrate at room temperature (around 20°C) for six days under constant shaking. After equilibration, the vials were centrifuged, and the supernatant was removed with a plastic Pasteur pipette and filtered through a 0.45  $\mu$ m reconstituted cellulose filter. After appropriate dilution, the contents of  $\gamma$ CD and HC were determined by HPLC-CAD. The vials containing the precipitate were weighted, dried *in vacuo* at 55°C for 5 hours and weighted again to calculate the mass loss and thereby the small amount of remaining supernatant that for practical reasons had not been separated from the precipitate. A fraction of the dry precipitate was dissolved and analyzed for its content of  $\gamma$ CD and HC by HPLC-CAD.

### 3.3 Quantification by HPLC-CAD

The total contents of  $\gamma$ CD and HC in the samples were quantified by HPLC connected to a Charged Aerosol Detector (CAD) (Corona Ultra RS, Dionex, Sunnyvale, CA) as previously described (Saokham and Loftsson, 2015). 70/30% V/V methanol/water was used as mobile phase and the analytes were separated on a C18 column thermostated at 30°C. The CAD was operating at 30°C. Three injections were made for each sample, and the standard deviation of the peak areas was in most cases below 1%. The standard curves for  $\gamma$ CD and HC were highly non-linear and were generated by fitting a function of the form  $y = a + bx^c$  to at least 8 data points in the range 0.05-4 mM for  $\gamma$ CD and 0.04-1.67 mM for HC.

### 3.4 Differential Scanning Calorimetry (DSC)

5-7 mg of the dry precipitates were precisely weighted out in aluminium crucibles, and thermograms were recorded on a DSC 214 (NETZSCH, Selb, Germany). Samples were heated from room temperature to 270°C at a rate of 20 K/min.

## 4. Results

### 4.1 Isothermal Titration Calorimetry

The calorimetric titrations of HC with  $\gamma$ CD were exothermic at all temperatures although the heat signals were small at 10°C but increased with increasing temperature. A single global fit of all calorimetric titrations was conducted with a binding model that assumes a single type of binding site on HC and assumes that the heat capacity change,  $\Delta C_p$ , is temperature-independent (Schönbeck et al., 2012). The fitting parameters are the stoichiometry,  $N$ , the binding constant at 20°C,  $K_{11}$ , the binding enthalpy at 20°C,  $\Delta H$ , and the change in heat capacity,  $\Delta C_p$ . As shown in Figure 2, this approach yielded good fits to all of the calorimetric data and provided precise binding parameters. The stoichiometry is close to unity, indicating the formation of 1:1 complexes.

Figure 2

### 4.2 Phase solubility studies

Plotting the equilibrium concentration of dissolved HC ( $S_{eq}$ ) as a function of the initial concentration of  $\gamma$ CD ( $L_t$ ) results in a  $B_S$ -type PS diagram (Figure 3) characterized by three well-defined regions. The plot of the equilibrium concentration of  $\gamma$ CD ( $L_{eq}$ ) (Figure 3) also has three regions. In region I, a linear increase in both  $S_{eq}$  and  $L_{eq}$  is observed. The intrinsic solubility of HC,  $S_0$ , was determined to  $0.728 \pm 0.006$  mM ( $n = 3$ ). The plateau in region II stretches from around 9 mM to 49 mM and is followed by region III where a strong decrease in  $S_{eq}$  and a strong increase in  $L_{eq}$  is observed. Peaking concentrations are observed for both  $S_{eq}$  and  $L_{eq}$  in the beginning of the plateau and are ascribed to super-saturation of the precipitating complex. If these peaks are ignored, the concentrations of HC and  $\gamma$ CD in region II are  $7.1 \pm 0.1$  mM and  $8.6 \pm 0.3$  mM, respectively.

Figure 3

From the length of the plateau in region II, the total amount of HC added to the vials, and the measured concentration of HC at the plateau, the stoichiometry of the precipitating entity is calculated (Higuchi and Connors, 1965) to be 1.43, or approximately 1.5  $\gamma$ CDs per HC.

Since the total amounts of HC and  $\gamma$ CD in the vials are known, the amounts in the precipitate can be calculated. The ratio of  $\gamma$ CD to HC in the precipitate is plotted in Figure 4. In region I, the precipitate presumably consists of pure undissolved HC while in region II two solid phases exist: pure undissolved HC and precipitated complex. The ratio of  $\gamma$ CD to HC increases in region II as solid HC is gradually converted into precipitated complex. In region III, the precipitate no longer contains a solid phase of pure HC so the relatively constant ratio shows that precipitation continues at a fixed stoichiometry around 1.6-1.7.

Figure 4

#### **4.3 Analysis of precipitate**

The amounts of HC and  $\gamma$ CD in the precipitate were analyzed by HPLC. Since it was impossible to remove all supernatant from the precipitate, the contributions from the remaining supernatant was corrected for by using the mass loss upon drying (from which the remaining volume of supernatant can be estimated) and the known concentrations in the supernatant. The results are also plotted in Figure 4 and agree well with the abovementioned indirect estimate of the composition of the precipitate.

The DSC thermogram of pure HC showed a melting peak at 228°C, which is close to a previously reported value of 223.3°C (Marciniec et al., 2003). This peak also appeared in the thermograms of precipitates from region I and II but not region III, confirming the assumption that a solid phase of pure HC is present in region I and II but not in region III. In principle, the amount of HC present as pure HC can be calculated from the area of the melting peak. Because the total amount of HC in the precipitate is already known, the amount of HC present as complexes can be calculated, and the stoichiometry of the precipitated complexes can be calculated throughout region II. Due to poor reproducibility, however, sufficiently precise values of the melting heats could not be obtained. Hence, no precise values of the stoichiometry of the precipitated complexes could be obtained in region II. Nevertheless, it was clear that the content of pure HC in the precipitate gradually decreased throughout region II in accordance with the assumptions described above.

## 5. Discussion

The PS diagram of the HC- $\gamma$ CD system is of the Bs-type. The conventional interpretation of such diagrams involves the precipitation of a poorly soluble complex. The results obtained in the present work clearly show that  $\gamma$ CD and HC precipitate in a ratio higher than 1:1 and most likely 1:1.5, suggesting the precipitation of  $\gamma$ CD:HC complexes with a 3:2 stoichiometry. The conclusion from the ITC analysis, however, strongly suggest that HC and  $\gamma$ CD form 1:1 complexes. It is therefore worth considering to what extent the 1:1 model can explain the data.

### 5.1 Compatibility with 1:1 binding model

If only 1:1 complexes contribute to the increase in solubility in region I, the 1:1 binding constant can be obtained from the slope,  $\alpha$ , of the initial linear part of the solubility curve and  $S_0$  (Higuchi and Connors, 1965):

$$K_{11} = \frac{\alpha}{(1-\alpha) \cdot S_0} \quad (5)$$

Since it is not clear exactly when region II starts, the calculation of the slope is only based on the solubility data where  $L_t$  is 0, 3.0, and 6.2. These data points lie perfectly on a straight line ( $r^2 = 0.99997$ ) with a slope that translates to  $K_{11} = 3.63 \text{ mM}^{-1}$ . This value is in good agreement with the ITC results, and the data in region I are thus compatible with a model where only 1:1 complexes are formed.

The 1:1 model predicts the relation between  $L_{eq}$  and  $S_{eq}$  in region II (and in region I) to be:

$$S_{eq} = S_0 + L_{eq} \cdot \frac{K_{11} \cdot S_0}{K_{11} \cdot S_0 + 1} \quad (6)$$

Using the value for the  $\gamma$ CD plateau as  $L_{eq}$ , the binding constant from ITC as  $K_{11}$ , and the measured  $S_0$ , yields  $S_t = 7.1 \text{ mM}$  which in excellent agreement with the observed value of the HC plateau in



region II. The heights of the HC and  $\gamma$ CD plateaus in region II are thus perfectly compatible with the 1:1 model but, as mentioned above, the length of region II clearly shows that the stoichiometry of the precipitating complexes is not 1:1. The data in region III are not compatible with a 1:1 model either. If the limited solubility of the 1:1 complex is the cause of the plateau in region II, the concentration in region III should theoretically stay above the height of the plateau minus  $S_0$  (Higuchi and Connors, 1965), which is around 6.4 mM. However, the concentration of HC in region III drops significantly below 6.4 mM and reaches a minimum of  $0.819 \pm 0.008$  mM at  $L_t = 140$  mM. These inadequacies of the 1:1 model are illustrated in Figure 5 where the predictions of the 1:1 model are plotted together with the experimental data.

Figure 5

## 5.2 Compatibility with 3:2 model

From the discussion above it is clear that the 1:1 model is insufficient to describe all of the observed features in region II and III. The experimental data indicate that  $\gamma$ CD and HC precipitate in a 3:2 ratio so it is natural to include 3:2 complexes in the mass balances. In the 1:1 model, it was assumed that the solutes precipitate due to the limited solubility of the formed 1:1 complexes but in the 3:2 model precipitation is caused by the limited solubility of the 3:2 complexes. Formation of 3:2 complexes may occur in a stepwise fashion, and a rigorous treatment should include all possible molecular species in the mass balances, i.e. complexes with 1:1, 1:2, 2:1, 2:2, and 3:2 stoichiometry. However, this would add considerable complexity to the model. For simplicity, the presently described 3:2 model considers only the presence of complexes with a 1:1 and 3:2 stoichiometry.

In principle, the experimental determination of both  $S_t$  and  $L_t$  in region II can be exploited to calculate the solubility of the 3:2 complex,  $S_{32}$ , and the additional equilibrium constant,  $K_{32}$ . To calculate  $S_{32}$  the mass balances in equations 1 and 2 are first modified by substituting  $[CD]$  with  $1/(K_{11} \cdot S_0)$ ,  $[S]$  with  $S_0$ , and  $[L_3S_2]$  with  $S_{32}$ :

$$S_{eq} = S_0 + [LS] + 2 \cdot S_{32} \quad (7)$$

$$L_{eq} = \varepsilon [LS] + 3 \cdot S_{32} \quad (8)$$

where  $\varepsilon = 1 + 1/(K_{11} \cdot S_0)$ . Subtracting  $\varepsilon \cdot S_{eq}$  from  $L_{eq}$  eliminates  $[LS]$  and allows  $S_{32}$  to be isolated:

$$S_{32} = \frac{L_{eq} - \varepsilon \cdot (S_{eq} - S_0)}{3 - 2\varepsilon} \quad (9)$$

Unfortunately, both the numerator and the denominator are calculated as differences between numbers that are similar in magnitude and thus become very small. Therefore, even small errors in the experimental values of  $L_{eq}$  and  $S_{eq}$  result in large errors in  $S_{32}$ . For example, if  $L_{eq} = 8.6$  mM and  $S_{eq} = 7.1$  mM, then  $S_{32} = 0.14$  mM. If  $L_{eq} = 8.9$  mM, then  $S_{32} = 1.1$  mM. With the current standard errors on  $L_{eq}$  and  $S_{eq}$  at the plateau no reliable estimate of  $S_{32}$  can be made.

To calculate  $K_{32}$ , the concentration of 3:2 complexes are eliminated from the mass balances in equations 1 and 2,  $[S]$  is substituted with  $S_0$ , and  $[L:S]$  is replaced by  $K_{11} \cdot S_0 [L]$ :

$$2 \cdot L_{eq} - 3 \cdot S_{eq} = 2 \cdot [L] \cdot (2 - K_{11} \cdot S_0) - 3 \cdot S_0 \quad (10)$$

From this,  $[L]$  can be isolated:

$$[L] = \frac{2 \cdot L_{eq} - 3 \cdot (S_{eq} - S_0)}{2 - K_{11} \cdot S_0} \quad (11)$$

This can then be inserted into the expression for  $K_{32}$ :

$$K_{32} = \frac{S_{32}}{S_0^2 \cdot [L]^3} \quad (12)$$

However, since  $S_{32}$  cannot be determined precisely neither can  $K_{32}$ . As an alternative equilibrium constant, the solubility product of the 3:2 complex,  $K_{32}^S$ , can be estimated without the use of  $S_{32}$ :

$$K_{32}^S = [L]^3 [S]^2 \quad (13)$$

In region II, [S] can be substituted with  $S_0$ :

$$K_{32}^S = [L]^3 \cdot S_0^2 \quad (14)$$

Using  $L_{eq} = 8.6$  mM,  $S_{eq} = 7.1$  mM,  $S_0 = 0.728$  mM, and  $K_{11} = 4.01$  mM<sup>-1</sup> in eq. 11 to calculate [L], we obtain from eq. 14 that  $K_{32}^S = 4.8$  mM<sup>5</sup>. It turns out (see below) that  $S_{32}$  must be very small and might even be zero. An imprecise value of  $S_{32}$  results in an imprecise value of  $K_{32}$ , and if the concentration of 3:2 complexes is zero, it does not make sense to define  $K_{32}$ . The solubility product,  $K_{32}^S$ , has the advantage that it does not require the presence of 3:2 complexes in the solution. It just assumes that  $\gamma$ CD and HC precipitate in a 3:2 ratio. It is worth noting that  $K_{32}^S$  can be expressed in terms of  $K_{32}$  and  $S_{32}$ .  $K_{32}^S = [L_3S_2] / K_{32}$  which in region II and III simplifies to  $K_{32}^S = S_{32} / K_{32}$ .

The predictions of the 3:2 model are shown in Figure 5. In general, it explains the experimental observations well except for the high concentrations in the beginning of region II which are ascribed to supersaturation. The low measured concentrations of HC at high CD concentrations ( $0.827 \pm 0.008$  mM at  $L_t = 140$  mM) require a low value of  $S_{32}$  as the predicted HC concentrations in region III are shifted upwards by  $2 \cdot S_{32}$ . Even though  $S_{32}$  is set to zero in Figure 5, the experimental data lie slightly below the predicted line.  $S_{32} = 0$  implies that the concentration of 3:2 complexes is always zero, and this simplifies the model such that  $K_{32}^S$  is the only adjustable parameter.  $S_0$  is measured directly and  $K_{11}$  is obtained from the ITC measurements. In Figure 5,  $K_{32}^S$  is chosen such that the predicted concentration of HC at the plateau matches the experimental value (7.1 mM). The good prediction of the remaining data in region III, with respect to both  $\gamma$ CD and HC, is a strong validation of the model.

The question remains what exactly precipitated from the solution? Since the experimental errors do not allow a firm conclusion to whether or not a 3:2 complex exists in solution, it seems a bit hasty

to assume the precipitation of a 3:2 complex. What seems to be certain is that  $\gamma$ CD and HC precipitate in a 3:2 ratio. This could be in the form of a 3:2 complex, a 4:6 complex or any other shape whose solubility product has the form  $[L]^{3 \cdot n} \cdot [S]^{2 \cdot n}$  because then  $[L]^3 \cdot [S]^2$  will be a constant. In principle,  $\gamma$ CD and HC could form a co-crystal of uncomplexed  $\gamma$ CD and HC but it could also be a co-crystal of 1:1 complexes and uncomplexed  $\gamma$ CD (in a 2:1 ratio). The possibilities are many.

Precipitation of 3:2  $\gamma$ CD complexes were previously reported for a range of steroid hormones, including hydrocortisone (Uekama et al., 1982). This conclusion was solely based on the length of the region II plateau of the PS diagram. The present study confirms this observation and further shows that the low solubility of this complex is responsible for the decrease in drug solubility in region III. Most of the HC in solution exists in the form of 1:1 complexes while the 3:2 complexes contribute very little to the HC solubility, if at all. It is worth noting that the 3:2 model accurately describes the experimentally determined PS diagrams of both HC and  $\gamma$ CD without introducing aggregates into the models. This suggests that aggregates have very little impact on the solubility of drug and CD, in contrast to previous speculations (Messner et al., 2011a; Saokham and Loftsson, 2017).

The present work provides a complete mechanistic model of the solubilisation of HC by  $\gamma$ CD and can therefore be used to make quantitative predictions regarding the solubility of HC in formulations with  $\gamma$ CD now that the parameters in the model have been determined ( $S_0 = 0.728$  mM,  $K_{11} = 4.01 \text{ mM}^{-1}$ ,  $K_{32}^S = 5.51 \text{ mM}^5$ ). This is exploited in the following section.

### 5.3 Implications for drug formulation:

The descending part of B<sub>S</sub>-type PS diagrams is of course problematic when trying to improve the aqueous solubility of a drug. The fact that the transition from region II to III is not fixed but depends on the initial amount of added drug only exacerbates the problem. From the PS diagram in Figure 3, one may falsely conclude that 40 mM of  $\gamma$ CD can dissolve 7.1 mM of HC but this is only the case if solid HC is present such that  $[S] = S_0$ . If all HC is dissolved, the system is in region III where a large excess of  $\gamma$ CD may cause significant amounts of HC to precipitate together with CDs. When testing the solubility of a drug in various media, excess amounts of drug are added to the solutions to obtain solutions that are saturated with drug. Such solubility experiments will therefore show that the solubility in a  $\gamma$ CD solution (e.g. 40 mM) is 7.1 mM. However, if one afterwards try to dissolve the amount of HC corresponding to 7.1 mM in 40 mM  $\gamma$ CD, a significant amount of HC will be found to precipitate with  $\gamma$ CD, and only a minor fraction will remain in solution (see Figure 6). In the latter case there is no excess of solid drug and therefore the system is in region III where  $S_{eq}$  will always be lower than the plateau value and decrease towards the solubility of the precipitating complex in the limit of very large surplus of CDs. If the precipitating complex is the same as the solubilizing complex the descending curve in region III is in general not a major problem as  $S_{eq}$  will not go below its plateau value minus  $S_0$ . This is the case for the 1:1 model as shown in Figure 5. But in the present case  $S_{eq}$  is limited by the solubility product,  $K_{32}^S$ , and goes towards zero with increasing  $L_t$ .

The negative effect of having too high a concentration of  $\gamma$ CD in the medium is shown in the reverse PS diagram in Figure 6 where the initial concentration of  $\gamma$ CD is set to 40 mM. It is seen that if 10 mM of HC is added to the solution less than 2 mM is solubilized, the rest is converted to precipitated 3:2 complex.

Figure 6

The inverse PS diagram in Figure 6 is constructed from the determined values of  $S_0$ ,  $K_{11}$ , and  $K_{32}^S$ . The detailed construction of reverse PS diagrams are described in the Supplementary material. Such a diagram is useful as it contains information on what happens when a given amount of drug is attempted dissolved in a dissolution medium containing a certain concentration of CD (40 mM  $\gamma$ CD in Figure 6). Will there be any precipitate and what will the precipitate consist of? The dissolution rate of solid HC may be different from solid 3:2 complex and therefore the composition of the precipitate may be important. Like the normal PS diagram the inverse PS diagram can be divided into different regions. In the first region, termed region IV, all of the added drug is dissolved since the product  $[L]^3 \cdot [S]^2$  is smaller than the solubility product,  $K_{32}^S$ . Therefore, there is no precipitate, and  $S_{eq}$  is given by a straight line with a slope of unity. Region IV continues until the point where  $[L]^3 \cdot [S]^2 = K_{32}^S$ , beyond which a fraction of the added HC will be converted to solid 3:2 complex. Since the precipitate only consists of solid 3:2 complex the system is in the above mentioned region III. At some point, when enough HC is added to the dissolution medium, there is not enough CD in the solution to convert all of the undissolved HC to solid 3:2 complex and the solid phase will consist of solid HC and solid 3:2 complex. At that point the system is in the above mentioned region II. Unlike the normal PS diagram, the first transition, from region IV to region III, is not fixed but depends on the concentration of CD in the medium. Higher CD concentrations cause the transition to occur at lower values of  $S_t$ .

For some purposes it may be desirable that the solution contains a maximum concentration of drug but no particles or precipitate. How can this be achieved? In region II where the precipitate consists

of solid complex and drug the solution contains the maximum amount of drug. Thus, if drug and CD are mixed in the amounts corresponding to their concentrations in region II there will be no precipitate at equilibrium. In the case of HC and  $\gamma$ CD at 20°C the amounts should correspond to 7.1 mM and 8.6 mM, respectively, to obtain a maximum concentration of HC and avoid any solid phase. Rather than mixing these exact amounts of drug and CD such a solution is more easily obtained by adding sufficient amounts of drug to the CD medium to ensure that solid drug and solid complex is present, followed by removal of the precipitate. The formulation at this point would not be very robust and very sensitive to variations in one of the two components, so the specification for the drug product should be carefully considered.

The descending part of the HC: $\gamma$ CD PS diagram descends to a very low concentration of HC and this poses a difficulty when using  $\gamma$ CD as a solubilizer for HC. But is it a general feature of  $\gamma$ CD that it forms B<sub>S</sub>-type diagrams where region III descends to such low values? If that is the case one should be very careful when using  $\gamma$ CD as a solubilizer as too high concentrations of  $\gamma$ CD results in very low concentrations of dissolved drug. An extensive study of the interaction between CDs and steroid hormones showed that natural  $\beta$ CD and  $\gamma$ CD formed B<sub>S</sub>-type PS diagrams with most of the hormones (Uekama et al., 1982). Judging from the length of the plateau region,  $\gamma$ CD precipitated in a 3:2 ratio with most of the hormones and thereby seemed to behave similar to the HC: $\gamma$ CD system. Care must therefore be taken when using  $\gamma$ CD as a solubilizer for this class of drugs although the CD may work very well for other classes of compounds. The present study clearly demonstrated the value of constructing a PS diagram when using CDs as a solubilizing excipient in order to define the optimal solubility and a robust formulation.

## 6. Conclusion

The solubility of hydrocortisone (HC) was measured in water containing varying concentrations of  $\gamma$ CD. The resulting B<sub>S</sub>-type phase-solubility diagram was described within the theoretical framework laid out by Higuchi and Connors. The initial linear increase in the solubility at low concentrations of  $\gamma$ CD was caused by the formation of a water-soluble 1:1 complex but the plateau was caused by precipitation of another entity with the stoichiometry 3:2  $\gamma$ CD:HC. The solubility product of the 3:2 entity quantitatively accounted for the decrease in HC solubility at high  $\gamma$ CD concentrations. Within the experimental errors it was not possible to conclude whether or not a 3:2  $\gamma$ CD:HC complex existed in solution at low concentrations.  $\gamma$ CD and HC may precipitate as larger units as long as the ratio of  $\gamma$ CD to HC is 3:2.

Care must be taken when co-formulating HC with natural  $\gamma$ CD as high concentrations of  $\gamma$ CD may severely reduce the amount of dissolved HC. Since steroid hormones seem to interact with  $\gamma$ CD in a similar manner this advice is extended to this class of drugs, but at present it is unclear whether it is a general feature of natural  $\gamma$ CD.

## Acknowledgements

Christian Schönbeck is supported by a grant (DFR – 5054-00173) from the Danish Council for Independent Research.



## References

- Higuchi, T., Connors, K.A., 1965. Phase-Solubility Techniques, in: Reilley, C. (Ed.), *Advances In Analytical Chemistry and Instrumentation*. Interscience, New York, pp. 117–212.
- Jansook, P., Kurkov, S. V., Loftsson, T., Taylor, M.J., Tanna, S., Sahota, T., 2010. Cyclodextrins as solubilizers: Formation of complex aggregates. *J. Pharm. Sci.* 99, 719–729.  
doi:<http://dx.doi.org/10.1002/jps.21861>
- Jansook, P., Loftsson, T., 2008.  $\gamma$ CD/HP $\gamma$ CD: Synergistic solubilization. *Int. J. Pharm.* 363, 217–219. doi:[10.1016/j.ijpharm.2008.07.011](https://doi.org/10.1016/j.ijpharm.2008.07.011)
- Marciniec, B., Kozak, M., Wachowski, L., Ogrodowczyk, M., 2003. Evaluation of radiostability of some steroid derivatives. *J. Therm. Anal. Calorim.* 73, 473–485.  
doi:[10.1023/A:1025465726691](https://doi.org/10.1023/A:1025465726691)
- Messner, M., Kurkov, S. V., Brewster, M.E., Jansook, P., Loftsson, T., 2011a. Self-assembly of cyclodextrin complexes: Aggregation of hydrocortisone/cyclodextrin complexes. *Int. J. Pharm.* 407, 174–183. doi:[10.1016/j.ijpharm.2011.01.011](https://doi.org/10.1016/j.ijpharm.2011.01.011)
- Messner, M., Kurkov, S. V., Palazón, M.M., Fernández, B.Á., Brewster, M.E., Loftsson, T., 2011b. Self-assembly of cyclodextrin complexes: Effect of temperature, agitation and media composition on aggregation. *Int. J. Pharm.* 419, 322–328. doi:[10.1016/j.ijpharm.2011.07.041](https://doi.org/10.1016/j.ijpharm.2011.07.041)
- Ryzhakov, A., Do Thi, T., Stappaerts, J., Bertolotti, L., Kimpe, K., Sá Couto, A.R., Saokham, P., Van den Mooter, G., Augustijns, P., Somsen, G.W., Kurkov, S., Inghelbrecht, S., Arien, A., Jimidar, M.I., Schrijnemakers, K., Loftsson, T., 2016. Self-Assembly of Cyclodextrins and Their Complexes in Aqueous Solutions. *J. Pharm. Sci.* 105, 2556–2569.  
doi:[10.1016/j.xphs.2016.01.019](https://doi.org/10.1016/j.xphs.2016.01.019)
- Saokham, P., Loftsson, T., 2017.  $\gamma$ -Cyclodextrin. *Int. J. Pharm.* 516, 278–292.  
doi:[10.1016/j.ijpharm.2016.10.062](https://doi.org/10.1016/j.ijpharm.2016.10.062)

- Saokham, P., Loftsson, T., 2015. A New Approach for Quantitative Determination of  $\gamma$ -Cyclodextrin in Aqueous Solutions: Application in Aggregate Determinations and Solubility in Hydrocortisone/ $\gamma$ -Cyclodextrin Inclusion Complex. *J. Pharm. Sci.* 104, 3925–3933.  
doi:10.1002/jps.24608
- Saokham, P., Sá Couto, A., Ryzhakov, A., Loftsson, T., 2016. The self-assemble of natural cyclodextrins in aqueous solutions: Application of miniature permeation studies for critical aggregation concentration (cac) determinations. *Int. J. Pharm.* 505, 187–193.  
doi:10.1016/j.ijpharm.2016.03.049
- Schönbeck, C., Holm, R., Westh, P., 2012. Higher order inclusion complexes and secondary interactions studied by global analysis of calorimetric titrations. *Anal. Chem.* 84, 2305–2312.  
doi:10.1021/ac202842s
- Uekama, K., Fujinaga, T., Hirayama, F., Otagiri, M., Yamasaki, M., 1982. Inclusion complexations of steroid hormones with cyclodextrins in water and in solid phase. *Int. J. Pharm.* 10, 1–15.  
doi:10.1016/0378-5173(82)90057-6
- Williams, H., Trevaskis, N., Charman, S., Shanker, R., Charman, W., Pouton, C., Porter, C., 2013. Strategies to address low drug solubility in discovery and development. *Pharmacol. Rev.* 65, 315–499. doi:10.1124/pr.112.005660
- Zughul, M., Badwan, A., 1998. SL2 type phase solubility diagrams, complex formation and chemical speciation of soluble species. *J. Incl. Phenom. Macrocycl.* ... 31, 243–264.  
doi:10.1023/A:1007965424219
- Zughul, M.B., 2007. Rigorous nonlinear regression analysis of phase solubility diagrams to obtain complex stoichiometry and true thermodynamic drug-cyclodextrin complexation parameters. *J. Incl. Phenom. Macrocycl. Chem.* 57, 525–530. doi:10.1007/s10847-006-9244-5
- Zughul, M.B., Badwan, A.A., 1997. Rigorous analysis of S2L-type phase solubility diagrams to

obtain individual formation and solubility product constants of both SL-and S2L-type complexes. *Int. J. Pharm.* 151, 109–119. doi:10.1016/S0378-5173(97)04901-6

Figures:

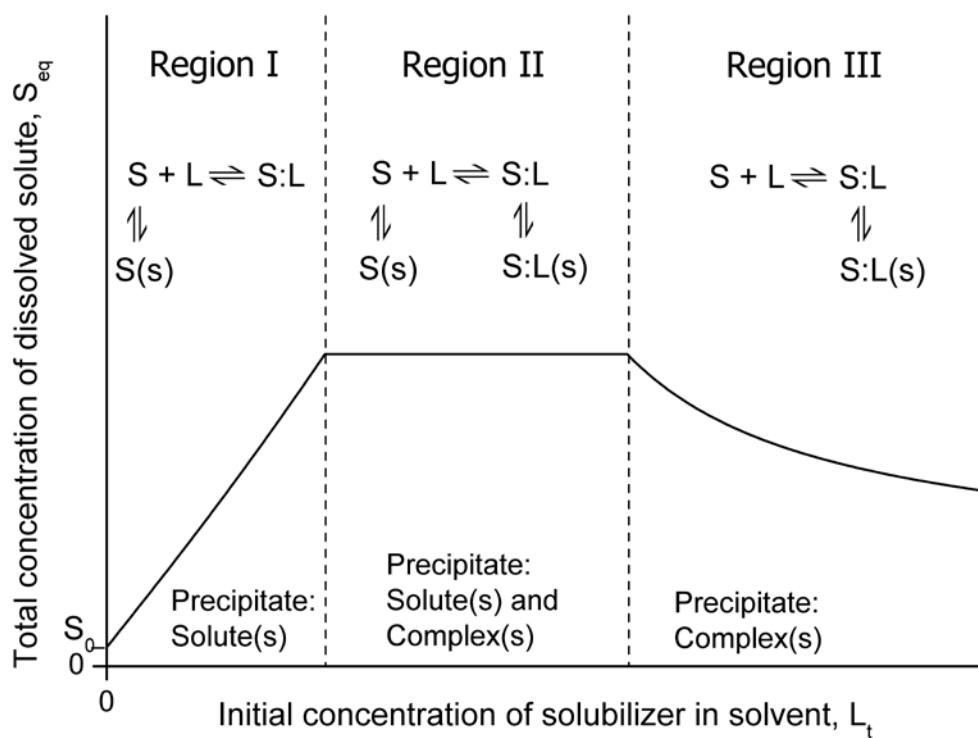
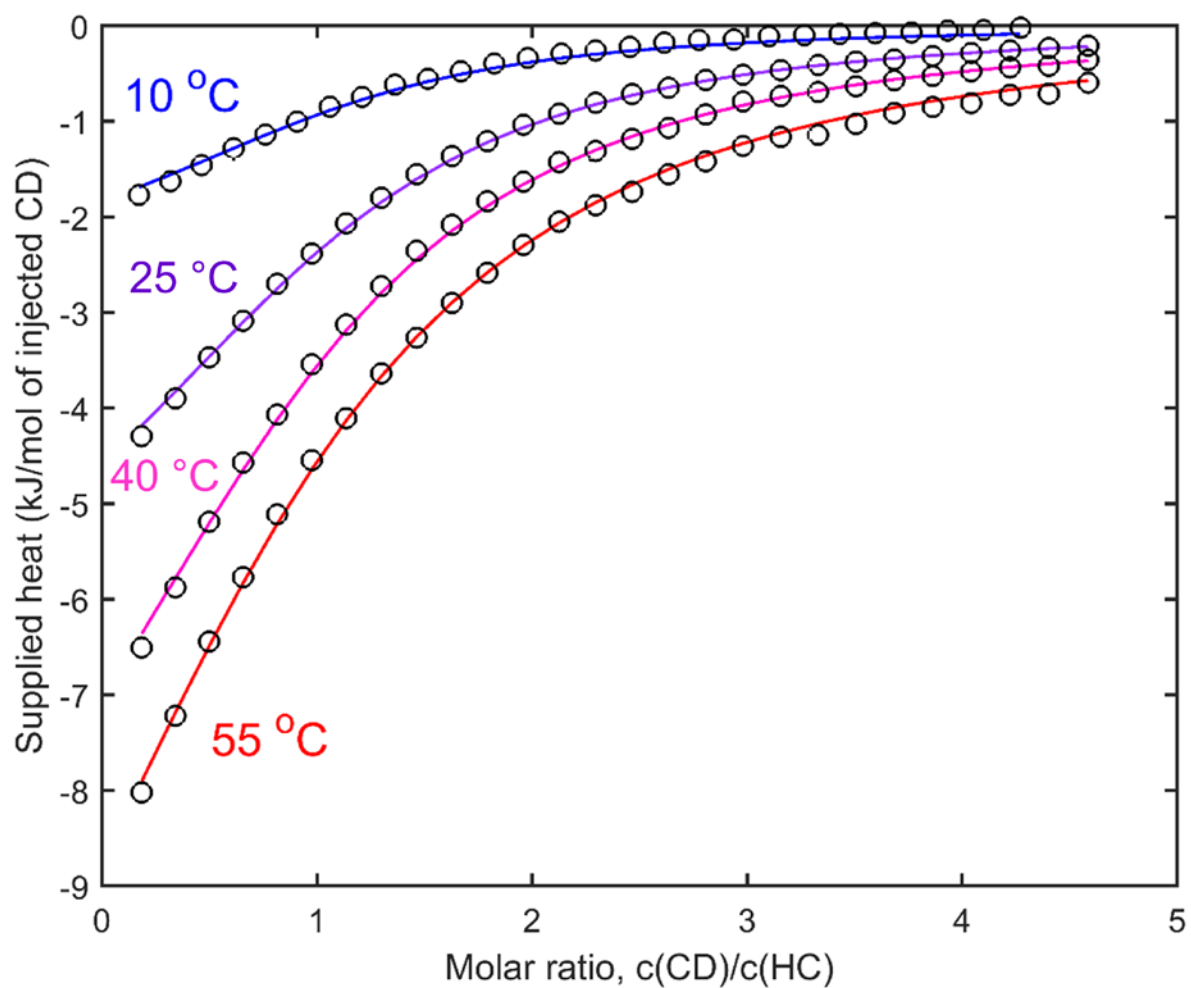


**Figure 1** Illustration of a Bs-type PS diagram.  $S_0$  is the intrinsic solubility of the drug. For each of the three regions the relevant equilibria and the composition of the precipitate are shown.  $S$ ,  $L$  and  $S:L$  denotes drug, ligand and complex in solution.



Parameter	Best fit value	Error at 95% CL	Correlation Matrix			
N	0.97	0.02	1.00	0.25	0.74	0.83
K at 20°C (M <sup>-1</sup> )	4010	84		1.00	0.56	0.58
ΔH at 20°C (kJ/mol)	-5.6	0.1			1.00	0.68
ΔC <sub>p</sub> (J/mol/K)	-294	6				1.00

**Figure 2** Global fit of 4 titrations of HC with  $\gamma$ CD in the range 10-55°C.

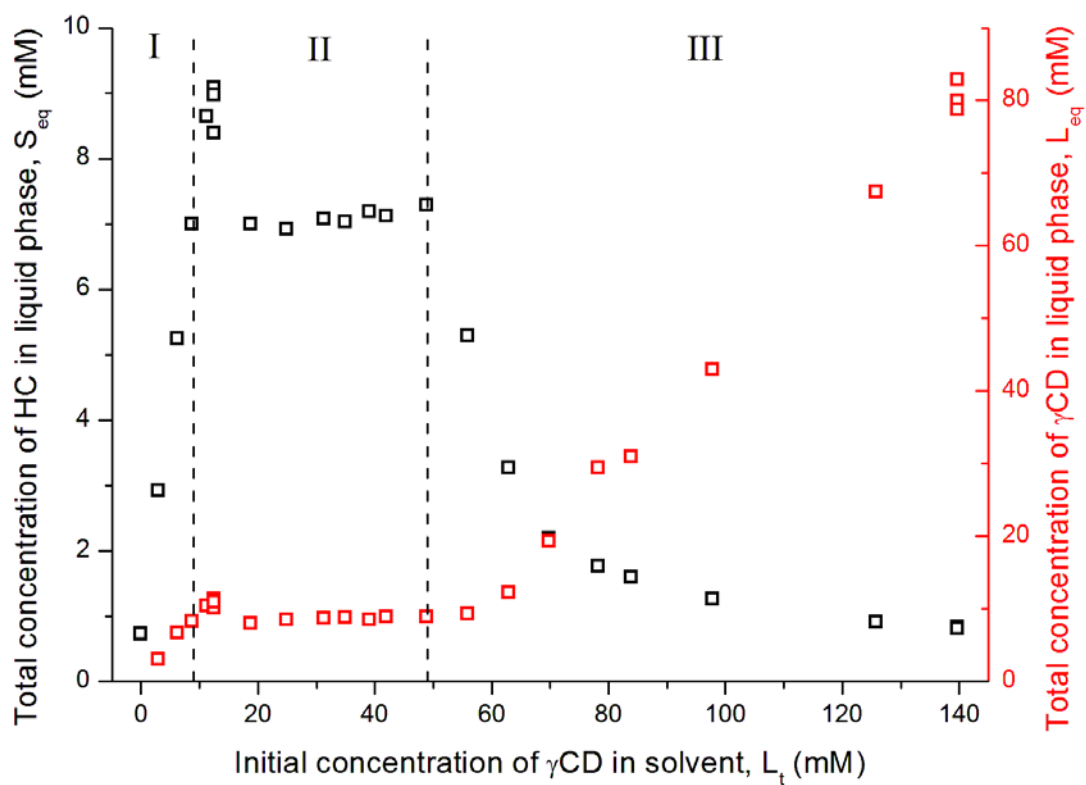


**Figure 3** Phase-solubility diagram of the HC- $\gamma$ CD system in water. Due to the different concentration ranges, the measured concentrations of HC and  $\gamma$ CD are given on the left and the right axis, respectively.

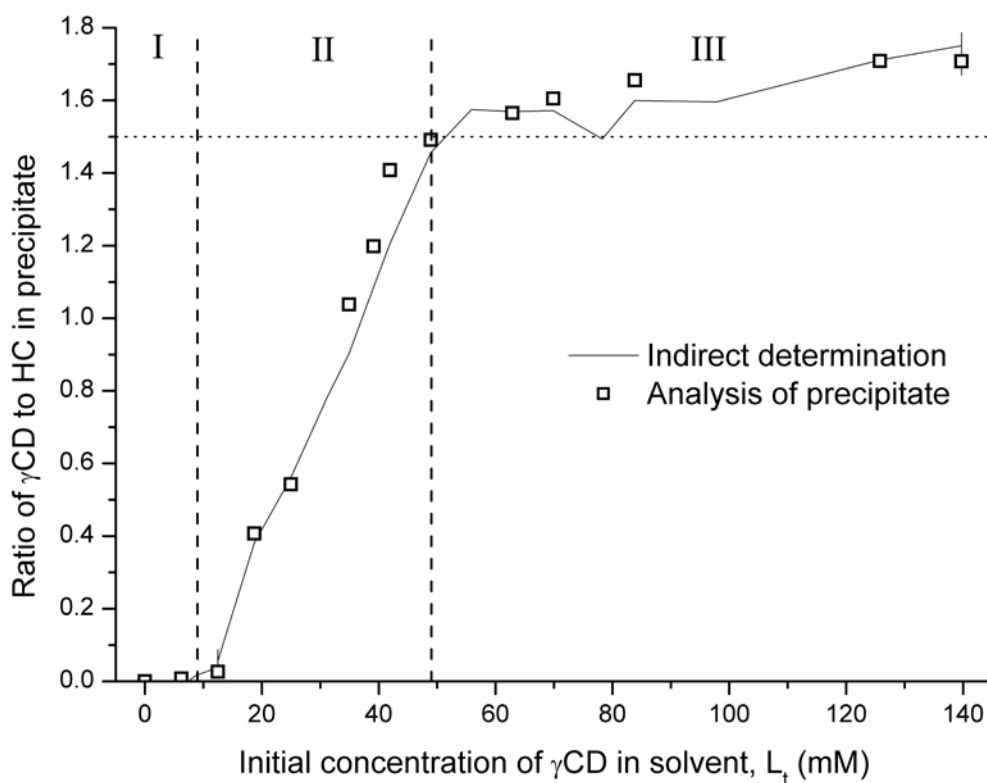


**Figure 4** Ratio of  $\gamma$ CD to HC in the precipitate from the phase-solubility study. The ratio was calculated indirectly by subtracting the measured concentrations in the solution phase from the total amounts, and was also determined directly by analysing the precipitate. The dotted horizontal line is a guide for the eye and has a value of 1.5.

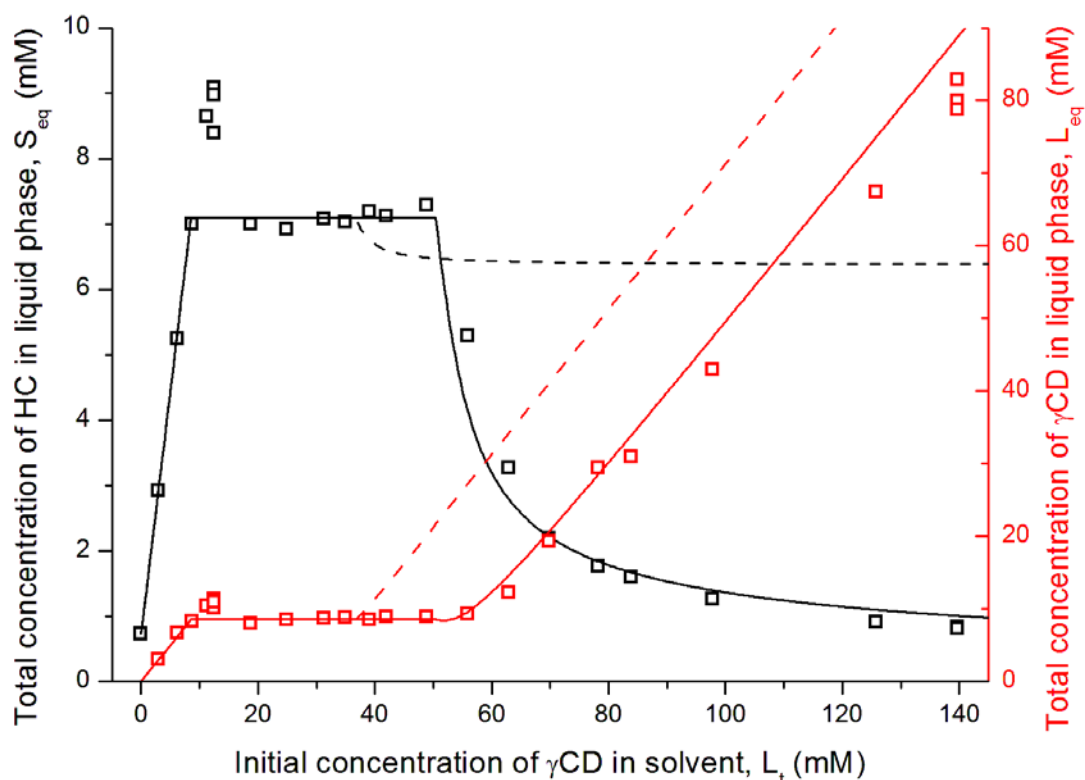


**Figure 5** Predictions of the 1:1 model (dotted lines) and the 3:2 model (solid lines) together with experimental data (open symbols). For the 1:1 model, the plotted functions are given in the Table 1. For the 3:2 model, the construction of the theoretical PS diagram is explained in the Supplementary material. In the 1:1 model, the used parameters were  $S_t = 35 \text{ mM}$ ,  $S_0 = 0.728 \text{ mM}$ ,  $S_{11} = 6.372 \text{ mM}$ , and  $K_{11} = 4.01 \text{ mM}^{-1}$ . The 3:2 model used the same values of  $S_t$ ,  $S_0$  and  $K_{11}$  in addition to  $K_{32}^S = 5.51 \text{ mM}^5$  and  $S_{32} = 0 \text{ mM}$ .



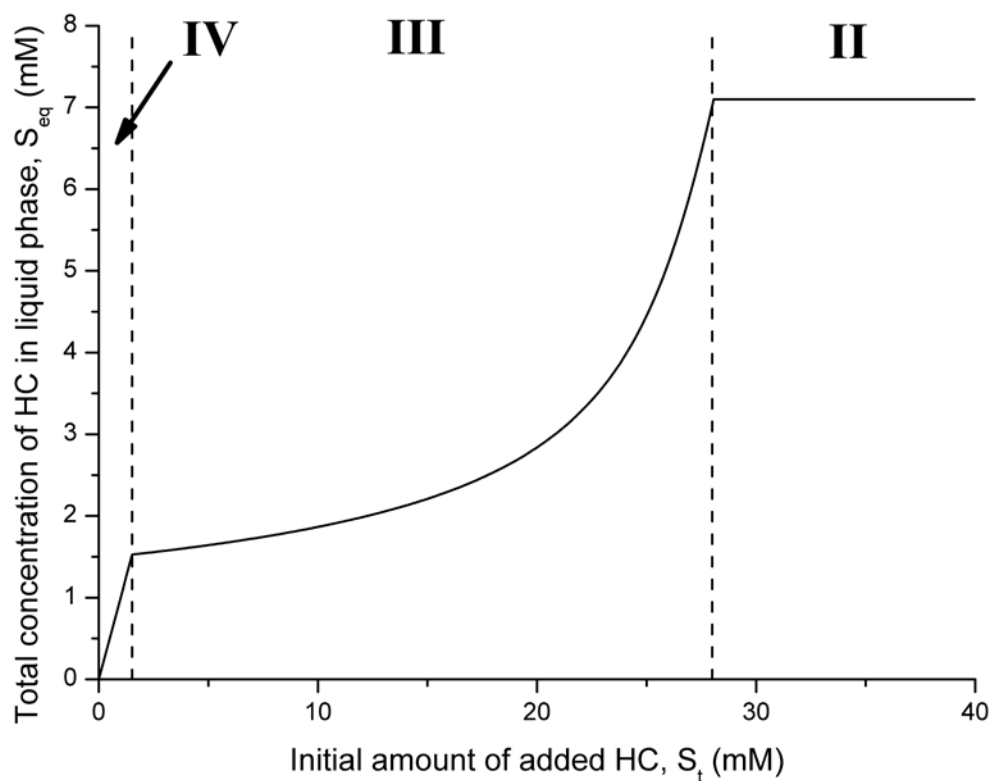


**Figure 6** The amount of HC in solution depends on the amount of added HC. The figure shows the predicted amount of dissolved HC as a function of the added amount of HC in the case where the dissolution medium initially contains 40 mM  $\gamma$ CD. It can be read from the plot that if 7.1 mM HC is added to a 40 mM  $\gamma$ CD solution only little more than 1.5 mM of HC will dissolve.